Development and Evaluation of Interleukin-2–Derived Radiotracers for PET Imaging of T Cells in Mice

Elly L. van der Veen[1], Frans V. Suurs[1], Frederik Cleeren[2], Guy Bormans[2], Philip H. Elsinga[3], Geke A.P. Hospers[1], Marjolijn N. Lub-de Hooge[3,4], Elisabeth G.E. de Vries[1], Erik F.J. de Vries[3], and Inês F. Antunes[3]

[1]Department of Medical Oncology, University Medical Center Groningen, University of Groningen, Groningen, The Netherlands; [2]Laboratory for Radiopharmaceutical Research, Department of Pharmacy and Pharmacology, University of Leuven, Leuven, Belgium; [3]Department of Nuclear Medicine and Molecular Imaging, University Medical Center Groningen, University of Groningen, Groningen, The Netherlands; and [4]Department of Clinical Pharmacy and Pharmacology, University Medical Center Groningen, University of Groningen, Groningen, The Netherlands

Recently, *N*-(4-^{18}F-fluorobenzoyl)-interleukin-2 (^{18}F-FB-IL2) was introduced as a PET tracer for T cell imaging. However, production is complex and time-consuming. Therefore, we developed 2 radiolabeled IL2 variants, namely aluminum ^{18}F-fluoride-(restrained complexing agent)-IL2 (^{18}F-AlF-RESCA-IL2) and ^{68}Ga-gallium-(1,4,7-triazacyclononane-4,7-diacetic acid-1-glutaric acid)-IL2 (^{68}Ga-Ga-NODAGA-IL2), and compared their in vitro and in vivo characteristics with ^{18}F-FB-IL2. **Methods:** Radiolabeling of ^{18}F-AlF-RESCA-IL2 and ^{68}Ga-Ga-NODAGA-IL2 was optimized, and stability was evaluated in human serum. Receptor binding was studied with activated human peripheral blood mononuclear cells (hPBMCs). Ex vivo tracer biodistribution in immunocompetent BALB/cOlaHsd (BALB/c) mice was performed at 15, 60, and 90 min after tracer injection. In vivo binding characteristics were studied in severe combined immunodeficient (SCID) mice inoculated with activated hPBMCs in Matrigel. Tracer was injected 15 min after hPBMC inoculation, and a 60-min dynamic PET scan was acquired, followed by ex vivo biodistribution studies. Specific uptake was determined by coinjection of tracer with unlabeled IL2 and by evaluating uptake in a control group inoculated with Matrigel only. **Results:** ^{68}Ga-Ga-NODAGA-IL2 and ^{18}F-AlF-RESCA-IL2 were produced with radiochemical purity of more than 95% and radiochemical yield of 13.1% ± 4.7% and 2.4% ± 1.6% within 60 and 90 min, respectively. Both tracers were stable in serum, with more than 90% being intact tracer after 1 h. In vitro, both tracers displayed preferential binding to activated hPBMCs. Ex vivo biodistribution studies on BALB/c mice showed higher uptake of ^{18}F-AlF-RESCA-IL2 than of ^{18}F-FB-IL2 in liver, kidney, spleen, bone, and bone marrow. ^{68}Ga-Ga-NODAGA-IL2 uptake in liver and kidney was higher than ^{18}F-FB-IL2 uptake. In vivo, all tracers revealed uptake in activated hPBMCs in SCID mice. Low uptake was seen after a blocking dose of IL2 and in the Matrigel control group. In addition, ^{18}F-AlF-RESCA-IL2 yielded the highest-contrast PET images of target lymph nodes. **Conclusion:** Production of ^{18}F-AlF-RESCA-IL2 and ^{68}Ga-Ga-NODAGA-IL2 is simpler and faster than that of ^{18}F-FB-IL2. Both tracers showed good in vitro and in vivo characteristics, with high uptake in lymphoid tissue and hPBMC xenografts.

Key Words: PET imaging; T cells; immunotherapy; interleukin-2; radiopharmaceuticals

J Nucl Med 2020; 61:1355–1360
DOI: 10.2967/jnumed.119.238782

Molecular imaging of immune cells for diagnosis and therapy evaluation in inflammatory and infectious diseases has been performed for decades (*1,2*). Now, interest in visualizing the immune response in cancer is also growing, as a result of the introduction of cancer immunotherapies. Immune checkpoint inhibitors have antitumor effects across several tumor types. However, not all patients respond, and some patients experience serious immune-related side effects. Therefore, strategies to select patients and optimize therapy are needed. Molecular imaging of immune cells might be a suitable method for patient selection, response prediction, and treatment evaluation in this context (*2*).

T cells are major players in both immune-related diseases and the tumor-immune response. During an immune response, T cells secrete the protein interleukin-2 (IL2). IL2 binds to the IL2 receptor (IL2-R), consisting of 3 subunits: IL2-Rα (CD25), IL2-Rβ (CD122), and IL2-Rγ (CD132) (*3–6*). Binding of IL2 to this complex leads to T-cell activation and differentiation (*3*). The IL2-R is expressed not only on activated cytotoxic T cells but also on other subpopulations, such as regulatory T cells. Specific binding of radiolabeled IL2 to T cells could be exploited for molecular imaging and might provide insight on immune responses.

Recombinant human IL2 binds to human and murine IL2-R and has been radiolabeled previously with SPECT isotopes such as ^{99m}Tc and ^{123}I (*7–9*). As PET offers better resolution than SPECT, the ^{18}F-labeled PET tracer *N*-(4-^{18}F-fluorobenzoyl)-IL2 (^{18}F-FB-IL2) was developed. ^{18}F-FB-IL2 PET imaging detected subcutaneously injected activated T cells and tumor infiltration of T cells in response to radiotherapy and immunization (*10–12*). Clinical trials with ^{18}F-FB-IL2 are ongoing. However, radiotracer production is complex, requiring 2.5 h and several synthesis modules. Moreover, the production yields sufficient radiotracer for only 1 or 2 patients (*13*). Therefore, we aimed to develop other radiolabeled IL2 PET tracers. First, we developed a simplified method for radiolabeling with ^{18}F, requiring fewer synthesis steps. Second, we used another PET isotope, ^{68}Ga, which is a generator-produced

Received Oct. 25, 2019; revision accepted Jan. 3, 2020.
For correspondence or reprints contact: Inês Farinha Antunes, Department of Nuclear Medicine and Molecular Imaging, University Medical Center Groningen, P.O. Box 30.001, 9700 RB Groningen, The Netherlands.
E-mail: i.farinha.antunes@umcg.nl
Published online Feb. 28, 2020.

radioisotope. Here, we present the development of aluminum ^{18}F-fluoride-(restrained complexing agent)-IL2 (^{18}F-AlF-RESCA-IL2) and ^{68}Ga-gallium-(1,4,7-triazacyclononane-4,7-diacetic acid-1-glutaric acid)-IL2 (^{68}Ga-Ga-NODAGA-IL2) (Fig. 1). To determine their potential for clinical use, in vitro and in vivo characteristics were evaluated and compared with ^{18}F-FB-IL2. For this purpose, in vitro binding assays with activated human peripheral blood mononuclear cells (hPBMCs) and ex vivo biodistribution studies on immunocompetent BALB/cOlaHsd (BALB/c) mice were performed. In addition, PET imaging and ex vivo biodistribution studies were performed on severe-combined immunodeficient (SCID) mice subcutaneously inoculated with activated hPBMCs.

MATERIALS AND METHODS

Production of ^{18}F-FB-IL2

The production method for ^{18}F-FB-IL2 has been described previously (*10*). This method was adapted to improve tracer yields (*13*).

Production of ^{18}F-AlF-RESCA-IL2

We developed a simplified method to label IL2 with ^{18}F, using the indirect ^{18}F-AlF-RESCA methodology, combining the chemical advantages of a chelator-based radiolabeling method with the unique physical properties of ^{18}F (*14–16*). ^{18}F-AlF was allowed to react with the RESCA-tetrafluorophenol ester ((±)-H_3RESCA-TFP) (Leuven University). Subsequently, the ^{18}F-AlF-RESCA complex was conjugated with IL2. The complete synthesis is described in the supplemental materials (available at http://jnm.snmjournals.org).

Production of ^{68}Ga-Ga-NODAGA-IL2

Our second strategy was radiolabeling of IL2 with ^{68}Ga. Because of the short half-life of ^{68}Ga, fewer synthesis steps and less synthesis time are required. First, 2,2′-(7-(1-carboxy-4-((2,5-dioxopyrrolidin-1-yl)oxy)-4-oxobutyl)-1,4,7-triazonane1,4-diyl)diacetic-acid (NODAGA-NHS) was conjugated to IL2, followed by radiolabeling with ^{68}Ga. We used 2 synthesis methods. In method 1, ^{68}Ga was eluted from the PS-H^+ cartridge in the cationic form (0.1 M HCl). However, large amounts of HCl are needed to efficiently elute all ^{68}Ga, leading to low concentrations of ^{68}Ga. Thus, for obtaining high concentrations of ^{68}Ga in a nonfractionated elution, we implemented method 2, in which ^{68}Ga was eluted from a PS-HCO_3 cartridge with deionized water (*17*). The complete synthesis methods are described in the supplemental materials.

In Vitro Binding Assays

In vitro binding to IL2-Rs was determined by performing binding assays with hPBMCs, isolated from peripheral blood from healthy volunteers by Ficoll-Paque Plus separation (GE Healthcare). Cells were kept in RPMI-1640 medium (Gibco) supplemented with 10% fetal calf serum. Isolated hPBMCs were activated by incubation with a 5 μg/mL concentration of phytohemagglutinin (Sigma-Aldrich) in a 5% CO_2 atmosphere at 37°C for 48 h (*10*). As a control, nonactivated hPBMCs were incubated for 48 h at 37°C and 5% CO_2. On the day of the experiment, another batch of hPBMCs was isolated, to compare CD25 (IL2-Rα) expression on these freshly isolated cells with expression on cells that had been incubated for 48 h.

Approximately 5×10^5 cells were incubated with 50 μL of tracer solution at 37°C for 30 min. The cells were washed twice with 1 mL of ice-cold phosphate-buffered saline (PBS) containing 1% human serum albumin (Sanquin). Activity in the cell fraction was measured in a γ-counter (Wizard^2 2480-0019, SW 2.1; PerkinElmer). Tracer uptake was corrected for the number of viable cells, which were counted manually using trypan blue. Uptake was expressed as percentage of cell-associated radioactivity per 500,000 cells. For ^{18}F-FB-IL2 and ^{18}F-AlF-RESCA-IL2, 4 independent experiments were performed, each experiment in triplicate. For ^{68}Ga-Ga-NODAGA-IL2, 2 independent experiments were performed, each experiment in triplicate.

In Vitro Stability Studies

The stability of ^{18}F-AlF-RESCA-IL2 and ^{68}Ga-Ga-NODAGA-IL2 was evaluated by adding 50 μL of tracer to 200 μL of human serum. The mixture was vortexed and incubated at 37°C for 60 and 120 min. After incubation, radiochemical purity was determined by a trichloroacetic acid precipitation assay (*18,19*).

Animal Studies

Animal studies were performed according to Dutch Regulations for Animal Welfare (IvD number 16395-01-007). The protocol was approved by the animal ethical committee of the University of Groningen. Animals were randomly assigned to different groups. A power calculation was performed to calculate the experimental group size. With an expected variation coefficient of 10%, a meaningful effect size of 25%, a confidence interval of 95%, and a power of 90%, a minimum of 5 animals per group is required. Therefore 5–6 animals were included in each group. Exclusion criteria were abnormal behavior, signs of sickness, more than a 15% reduction in body weight, and death.

Biodistribution Studies and In Vivo Stability in BALB/c Mice. Ex vivo biodistribution studies were performed on immunocompetent BALB/c mice 5–8 wk old (Envigo). The weights of the animals were comparable. Tracer (150 μL) was injected via the penile vein: 4.20 ± 0.8 MBq (0.75 ± 0.22 μg) of ^{18}F-FB-IL2; 1.21 ± 0.95 MBq (0.25 ± 0.24 μg) of ^{18}F-AlF-RESCA-IL2; and 0.55 ± 0.13 MBq (0.32 ± 0.18 μg) of ^{68}Ga-Ga-NODAGA-IL2 (method 1). The mice were sacrificed at 15, 60. and 90 min after injection (6 mice per time point). Organs were dissected and counted in a γ-counter. Bone marrow was isolated from the hind limb long bones (femurs and tibias) via centrifugation. Uptake in organs was calculated as percentage injected dose per gram of tissue. Total injected dose was determined by measuring activity in the syringe before and after injection. In vivo stability was determined in plasma samples by a trichloroacetic acid precipitation assay.

PET Imaging and Ex Vivo Biodistribution in SCID Mice with a hPBMC Xenograft. PET studies were performed on Fox Chase severe combined immunodeficient (SCID) beige mutant mice 5–8 wk old (Envigo). The mice were subcutaneously implanted with 10×10^6 48-h phytohemagglutinin–activated hPBMCs in 300 μL of 1:1 PBS:Matrigel (Corning) in the right shoulder. As a negative control group, mice were subcutaneously inoculated with Matrigel only. Tracer was injected via the penile vein 15 min after inoculation: 1.17 ± 0.62 MBq (0.15 ± 0.11 μg) of ^{18}F-FB-IL2; 2.10 ± 2.41 MBq (0.18 ± 0.12 μg) of ^{18}F-AlF-RESCA-IL2; and 0.44 ± 0.18 MBq (0.26 ± 0.13 μg) of ^{68}Ga-Ga-NODAGA-IL2 (method 2). For blocking experiments, a third group inoculated with 10×10^6 phytohemagglutinin-activated hPBMCs received a coinjection of tracer with a blocking dose of unlabeled IL2

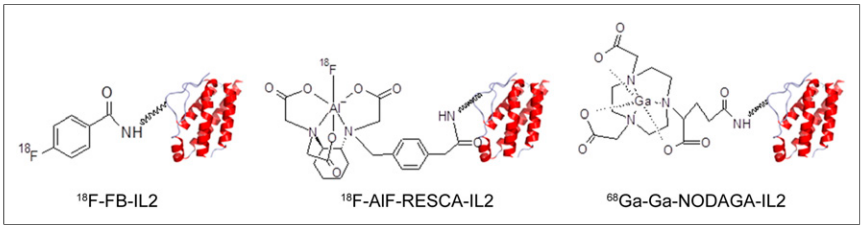

FIGURE 1. Structures of radiolabeled IL2 PET tracers.

(100 μg). Directly after tracer injection, a 60-min dynamic PET scan was made using a Focus 220 PET scanner (CTI Siemens), followed by a 15-min transmission scan with a ^{57}Co point source to correct for tissue attenuation, random coincidences, and scatter. After the scan, the mice were sacrificed and organs were dissected and counted in a γ-counter. During all scans and invasive procedures, the mice were anesthetized with isoflurane and medical air inhalation anesthesia (5% induction, 2.5% maintenance).

PET Reconstruction

PET data were reconstructed into 6 frames and corrected for radioactive decay, random coincidences, scatter, and attenuation. Reconstructed images were analyzed using PMOD software (version 3.9; PMOD Technologies LCC). Three-dimensional regions of interest were drawn around the site of cell inoculation. For other organs, a fixed-size sphere was drawn on representative parts of the organs. PET data are presented as percentage injected dose per gram of tissue.

FACS Analysis

The CD25 (IL2-Rα) expression on hPBMCs was determined by fluorescence-activated cell sorting (FACS) analysis. For in vitro experiments, hPBMCs were washed once with 3 mL of ice-cold PBS and resuspended in 500 μL of PBS. To select viable cells, 5 μL of Zombie Aqua (Biolegend) were added and incubated in the dark at room temperature for 15 min. The cells were washed with PBS containing 5% fetal calf serum and were resuspended in PBS containing 2% fetal calf serum (FACS buffer), to a concentration of 1×10^6 cells/mL. To 0.1 mL of cell suspension, 5 μL of either fluorescein isothiocyanate–conjugated mouse antihuman antibody CD25 (ImmunoTools) or mouse fluorescein isothiocyanate–IgG (BD Biosciences) as a control were added. Then, 5 μL of phycoerythrin-conjugated antihuman CD3 antibody (eBioscience) were added and the cells were incubated for 45 min on ice. Afterward, the cells were washed twice with 3 mL of cold FACS buffer and resuspended in 0.1 mL of FACS buffer. FACS measurements were performed on a BD FACSVerse apparatus (BD Biosciences). FACS data were analyzed using Flow-Jo software (version 10). Cells were gated for living cells, followed by CD3-positive cells. In this population, the percentage of CD25-positive cells was selected. For in vivo experiments, hPBMC activation was confirmed by FACS analysis of CD25 only.

Statistical Analysis

Data are presented as mean ± SD. Groups were compared using an unpaired 2-tailed *t* test (in vitro binding data and stability data) or a Bonferroni-corrected Mann–Whitney *U* test (PET imaging and biodistribution data) (GraphPad Prism, version 7.0). *P* values of 0.05 or less were considered statistically significant.

RESULTS

Production of ^{18}F-FB-IL2

^{18}F-FB-IL2 was obtained with a radiochemical yield of 1.0% ± 0.4%, a molar activity of 342 ± 385 GBq/μmol, and a radiochemical purity of more than 95% within 150 min.

Production of ^{18}F-AlF-RESCA-IL2

In the first step, the ^{18}F-AlF-RESCA-TFP complex was formed at room temperature with high yield (radiochemical yield > 80%). The subsequent conjugation of IL2 with ^{18}F-AlF-RESCA-TFP provided the final product, ^{18}F-AlF-RESCA-IL2, with a radiochemical yield of 2.4% ± 1.6%, a molar activity of 910 ± 927 GBq/μmol, and a radiochemical purity of more than 95% within 90 min.

Production of ^{68}Ga-Ga-NODAGA-IL2

The conversion of NODAGA-IL2 into ^{68}Ga-Ga-NODAGA-IL2 according to method 1 resulted in almost quantitative yields (85% ± 29%) when small volumes (100–200 μL, 20–100 MBq) of freshly eluted ^{68}Ga-Cl_3 were used. When large volumes (1 mL, 200–600 MBq) were used, the yields dropped to 6.0% ± 6.6%.

Labeling of NODAGA-IL2 with small volumes (200 μL, 200–600 MBq) of freshly eluted ^{68}Ga-Cl_3 according to method 2 resulted in ^{68}Ga-NODAGA-IL2 with a radiochemical yield of 13.1% ± 4.7%, a molar activity of 76 ± 34 GBq/μmol, and a radiochemical purity of more than 91% within 60 min.

In Vitro Binding Assays

^{18}F-AlF-RESCA-IL2 uptake in activated hPBMCs (73% ± 27.6%) was substantially higher than uptake of ^{18}F-FB-IL2 (4.8% ± 2.8%, $P = 0.015$) or ^{68}Ga-Ga-NODAGA-IL2 (12.7% ± 0.1%, $P = 0.019$) (Fig. 2A). When we compared activated-to-nonactivated ratios, we found that the new tracers were just as selective as ^{18}F-FB-IL2 (Fig. 2B). All tracers showed a reduction in cell binding in fresh and nonactivated hPBMCs, compared with uptake in activated hPBMCs. More CD3-positive T cells expressed CD25 in the activated hPBMCs than in the incubated nonactivated hPBMCs (32.1% ± 6.0% vs. 3.4% ± 2.1%, $P = 0.002$) or in the freshly isolated hPBMCs (3.1% ± 1.2%, $P = 0.001$) (Supplemental Fig. 1).

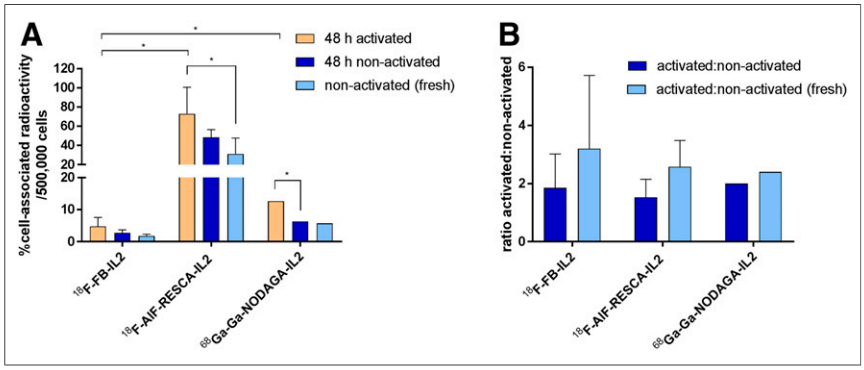

FIGURE 2. In vitro binding assay in human PBMCs for ^{18}F-FB-IL2, ^{18}F-AlF-RESCA-IL2, and ^{68}Ga-Ga-NODAGA-IL2. Four independent experiments were performed for ^{18}F-FB-IL2 and ^{18}F-AlF-RESCA-IL2, in triplicate; For ^{68}Ga-Ga-NODAGA-IL2, 2 independent experiments were performed, in triplicate. (A) Data expressed as percentage of cell-associated radioactivity per 500,000 cells. (B) Data expressed as ratio of activated to nonactivated cells. Data are mean ± SD. *$P \leq 0.05$.

In Vitro Stability Studies

^{18}F-AlF-RESCA-IL2 and ^{68}Ga-Ga-NODAGA-IL2 showed comparable high stability in human serum, with more than 90% of both tracers remaining intact after 1 and 2 h (Fig. 3). For comparison, ^{18}F-FB-IL2 showed slightly higher stability (100% at 1 and 2 h, as described earlier (*10,11*)).

Animal Studies

Ex Vivo Biodistribution Studies in Immunocompetent Mice. Ex vivo biodistribution studies showed high uptake of ^{18}F-FB-IL2 at sites of renal excretion (Fig. 4; Supplemental Table 1). After 15 min, kidney uptake of ^{18}F-AlF-RESCA-IL2 was higher than

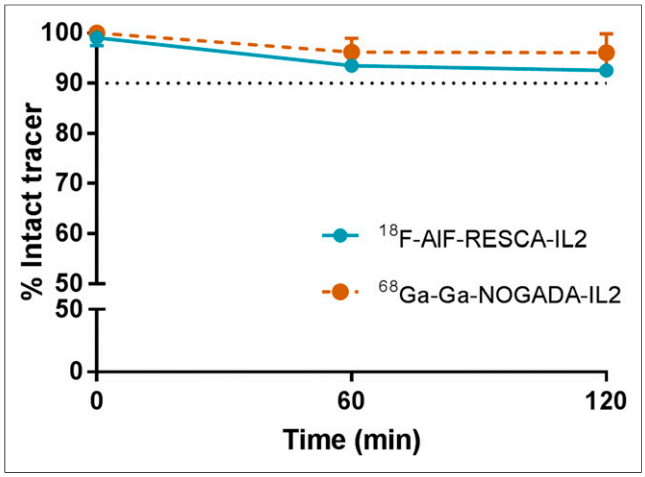

FIGURE 3. In vitro stability studies in human serum for ^{18}F-AlF-RESCA-IL2 and ^{68}Ga-Ga-NODAGA-IL2. Data are expressed as percentage of intact tracer after 60 and 120 min of incubation (mean ± SD).

that of ^{18}F-FB-IL2 (P = 0.009) (Supplemental Table 1). However, activity in urine was higher for ^{18}F-FB-IL2 (P = 0.004), indicating faster renal excretion. At 60 and 90 min after injection, ^{18}F-AlF-RESCA-IL2 showed higher uptake than ^{18}F-FB-IL2 in liver, kidney, spleen, bone, and bone marrow. ^{68}Ga-Ga-NODAGA-IL2 showed a biodistribution pattern comparable to that of ^{18}F-AlF-RESCA-IL2, with high uptake in liver and kidney. Moreover, ^{68}Ga-Ga-NODAGA-IL2 uptake in the kidney was higher than either ^{18}F-FB-IL2 or ^{18}F-AlF-RESCA-IL2 uptake at all time points (Fig. 4). ^{18}F-AlF-RESCA-IL2 showed the highest uptake in lymphoid organs, such as spleen, lymph nodes, and bone marrow, at 60 min and 90 min.

In vivo stability of ^{18}F-AlF-RESCA-IL2 was comparable to that of ^{18}F-FB-IL2 at 90 min after injection (81% ± 9% for ^{18}F-FB-IL2 vs. 72% ± 9% for ^{18}F-AlF-RESCA-IL2, P = 0.058) (Supplemental Fig. 2). ^{68}Ga-Ga-NODAGA-IL2 was less stable than ^{18}F-FB-IL2 at 90 min after injection (^{68}Ga-Ga-NODAGA-IL2, 65% ± 5%; P = 0.003).

PET Imaging and Ex Vivo Biodistribution in SCID Mice with a hPBMC Xenograft. Activated hPBMC xenografts inoculated in SCID mice were visualized with all tracers by dynamic PET imaging. No uptake was observed in the Matrigel control group or after coinjection of tracer with a blocking dose of unlabeled IL2. PET images of all tracers showed high uptake in liver and kidney, which did not substantially change over time.

With ^{18}F-FB-IL2 PET, lymph nodes could be detected in only 3 of 5 mice (Fig. 5A), whereas ^{18}F-AlF-RESCA-IL2 PET could clearly visualize lymph nodes in all mice at 60 min after injection (Fig. 5B). With ^{68}Ga-Ga-NODOGA-IL2 PET, lymph nodes could be detected as well, although not as clearly as with ^{18}F-AlF-RESCA-IL2 PET (Fig. 5C).

The PET results were confirmed by ex vivo studies showing higher uptake in activated PBMCs than in Matrigel control for all tracers (Fig. 6; Supplemental Table 2). A blocking dose of unlabeled IL2 reduced tracer uptake in PBMCs, with the largest reduction being for ^{18}F-AlF-RESCA-IL2 (^{18}F-FB-IL2, 43.2%; ^{18}F-AlF-RESCA-IL2, 67.5%; ^{68}Ga-Ga-NODAGA-IL2, 26.9%).

DISCUSSION

We developed 2 radiolabeled IL2 tracers, namely ^{18}F-AlF-RESCA-IL2 and ^{68}Ga-Ga-NODAGA-IL2. Both tracers could be produced consistently with a shorter production time than for ^{18}F-FB-IL2. Although labeling of ^{18}F-AlF-RESCA-IL2 gives decay-corrected radiochemical yields similar to those for ^{18}F-FB-IL2, the practical amounts of ^{18}F-AlF-RESCA-IL2 produced are 50% higher because of the shorter production time. In addition, the production requires only 1 synthesis module. This is an advantage for clinical use, as more production runs could be planned and, thus, more patients scanned. The radiochemical yield of ^{68}Ga-Ga-NODAGA-IL2 strongly depends on the volume in which $^{68}GaCl_3$ can be obtained. An advantage of this tracer is that no cyclotron is needed for radioisotope production, allowing production at sites without a cyclotron.

RESCA was chosen as the chelator for incorporation of Al^{18}F because the complex can be formed at room temperature, preventing potential degradation of the IL2 protein at higher temperatures. Although RESCA was successfully conjugated to IL2, most of the direct radiolabeling attempts did not yield any product, most likely because of the substantial loss of RESCA-IL2 conjugate in the tC2 cartridge during purification. Therefore, it was decided to use an indirect radiolabeling method. This approach provided the desired product, although at a low radiochemical yield of 2.4% ± 1.6%. Nevertheless, starting with less than 50 GBq allows production of a quantity of ^{18}F-AlF-RESCA-IL2 sufficient for several patients (1,375 ± 791 MBq; recommended injected dose, 200 MBq).

For the ^{68}Ga-based IL2 tracer, NODAGA was chosen as the chelator because it has a

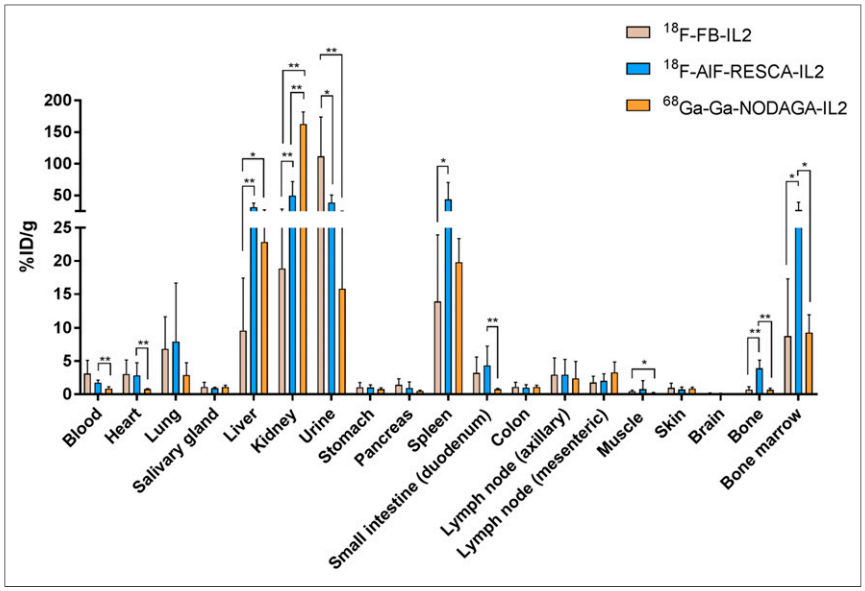

FIGURE 4. Comparison of ex vivo biodistribution in immunocompetent BALB/c mice 60 min after injection between ^{18}F-FB-IL2, ^{18}F-AlF-RESCA-IL2, and ^{68}Ga-Ga-NODAGA-IL2 (n = 6 per tracer). Uptake is expressed as percentage injected dose per gram of tissue (%ID/g, mean ± SD). *$P \leq 0.05$. **$P \leq 0.01$.

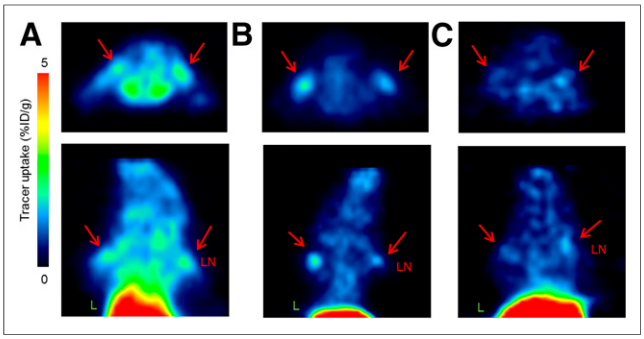

FIGURE 5. Representative PET images in immunodeficient SCID mice inoculated with activated PBMCs or Matrigel control in right shoulder 15 min before tracer injection for ^{18}F-FB-IL2 (A), ^{18}F-AlF-RESCA-IL2 (B), and ^{68}Ga-Ga-NODAGA-IL2 (C). Clear lymph node uptake is depicted by arrows. Upper panel shows transaxial view; lower panel shows coronal view. L = liver; LN = lymph node; %ID/g = percentage injected dose per gram of tissue.

smaller coordination pocket forming more stable complexes with ^{68}Ga. Moreover, it allows labeling with ^{68}Ga at room temperature (*20,21*). During ^{68}Ga-Ga-NODAGA-IL2 production, the addition of higher amounts of ^{68}Ga-Cl_3 led to yields of less than 10%. A plausible explanation is the low amounts of protein remaining after conjugation, as most of the conjugated NODAGA-IL2 is lost during tC2 purification. With these low radiochemical yields and a maximum amount of 1 GBq eluted from the ^{68}Ge/^{68}Ga generator, ^{68}Ga-Ga-NODAGA-IL2 becomes less suitable for clinical use, since it would be difficult to reliably obtain a patient dose. Therefore, to use ^{68}Ga-Ga-NODAGA-IL2 in clinical studies, further optimization is warranted.

Our study showed that ^{18}F-AlF-RESCA-IL2 had the highest in vitro uptake in hPBMCs and the highest in vivo uptake in target tissues of BALB/c mice, such as lymph nodes, spleen, and bone marrow. Since IL2 is injected in a subpharmacologic dose, no adverse effects are expected. In addition, in the first clinical study with ^{18}F-FB-IL2, no adverse effects due to radiation burden were observed. Therefore, we do not expect additional toxicity from the new analogs. In contrast to ^{18}F-FB-IL2 and ^{68}Ga-Ga-NODAGA-IL2, which have mainly renal clearance, ^{18}F-AlF-RESCA-IL2 has higher hepatobiliary clearance, as can be attributed either to the presence of the RESCA moiety, which introduces an additional charge, or to the presence of degradation products, such as unconjugated ^{18}F-AlF-RESCA or free ^{18}F-AlF (*16,22*). These high uptake values obtained in excretory organs are in the same range as obtained with previous IL2-based tracers, for which no renal or hepatic toxicity was found (*23–25*). A limitation for clinical use of ^{68}Ga-Ga-NODAGA-IL2 is high retention in the kidney, which can lead to a radiation burden due to its increased positron energy compared with ^{18}F-fluorine. Therefore, ^{18}F-AlF-RESCA-IL2 might be preferred for clinical molecular imaging studies. PET images obtained with ^{18}F-AlF-RESCA-IL2 showed less background and therefore were of higher contrast than images obtained with the other tracers. In addition, lymph nodes could be visualized with ^{18}F-AlF-RESCA-IL2 in all animals, whereas with ^{18}F-FB-IL2 PET, lymph nodes were visible in only some animals, indicating ^{18}F-AlF-RESCA-IL2 to have good targeting characteristics.

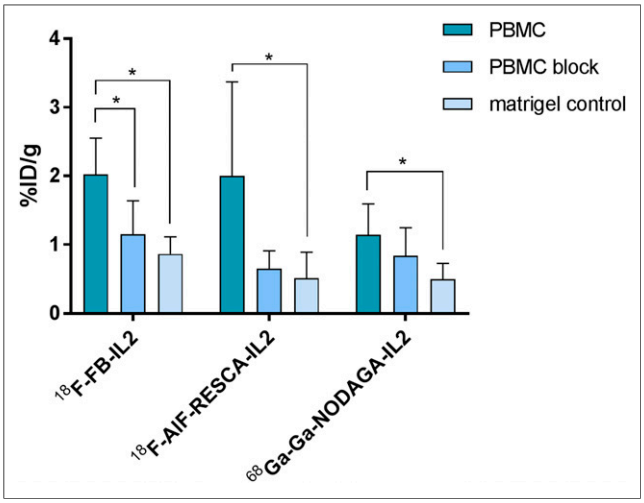

FIGURE 6. Ex vivo uptake (percentage injected dose per gram of tissue [%ID/g]) of 3 radiolabeled IL2 variants in mice inoculated with activated PBMCs or Matrigel control in right shoulder 15 min before tracer injection. For blocking, excess of unlabeled IL2 was coinjected with radiolabeled IL2 (PBMC block). ^{18}F-FB-IL2: PBMC, n = 4; PBMC block, n = 6; Matrigel control, n = 5. ^{18}F-AlF-RESCA-IL2: PBMC, n = 5; PBMC block, n = 6; Matrigel control, n = 6. ^{68}Ga-Ga-NODAGA-IL2: PBMC, n = 5; PBMC block, n = 6; Matrigel control, n = 5. Data are expressed as mean ± SD. *$P \leq 0.05$.

Previous SPECT and PET imaging studies have shown that IL2-derived tracers could detect T cells in inflammatory and infectious diseases, as well as in different tumor types (*7–9*, *23–28*). In a small clinical pilot study on only 5 patients with melanoma, ^{99m}Tc-IL2 SPECT could detect metastases (*29*). Currently, other tracers targeting immune cells are also being developed, such as targeting T cells via CD8-specific tracers (*30–33*). Another method to detect immune cells is radiolabeling of immune checkpoint–targeting monoclonal antibodies with long–half-life isotopes such as ^{89}Zr. Compared with these antibody-based tracers, radiolabeled IL2 tracers have an advantage in that, with shorter half-lives, imaging can be performed shortly after tracer injection. Thus, in a fast, noninvasive manner, information about the presence and dynamics of immune cells can be gained. Our results indicate that ^{18}F-AlF-RESCA-IL2 has good in vitro and in vivo characteristics and the potential to be used as a PET tracer for imaging of T cells.

CONCLUSION

We developed 2 radiolabeled IL2 tracers for imaging of immune cells: ^{18}F-AlF-RESCA-IL2 and ^{68}Ga-Ga-NODAGA-IL2. Production of these tracers was faster than production of the previously developed ^{18}F-FB-IL2 and is a potential advantage for clinical use. ^{18}F-AlF-RESCA-IL2 showed the highest practical production yield and the highest in vitro binding to activated hPBMCs. Moreover, in vivo studies showed high uptake of ^{18}F-AlF-RESCA-IL2 in PBMC xenografts and lymphoid tissues such as spleen, bone marrow, and lymph nodes. This finding supports the potential to use this tracer in future studies for detection of CD25-positive immune cells.

DISCLOSURE

The research leading to these results received funding from the Innovative Medicines Initiatives 2 Joint Undertaking under grant agreement No. 116106 (TRISTAN). This Joint Undertaking receives support from the European Union's Horizon 2020 research and innovation program and EFPIA. Elisabeth de Vries had a consulting

and advisory role for NSABP, Daiichi Sankyo, Pfizer, Sanofi, Merck, and Synthon Biopharmaceuticals; and received grants from Amgen, Genentech, Roche, Chugai Pharma, CytomX Therapeutics, Nordic Nanovector, G1 Therapeutics, AstraZeneca, Radius Health, and Bayer, all made available to the institution, outside the submitted work. Erik de Vries received grants from ZonMW (95104008 and 95105010) during this study; received a grant from the Dutch Cancer Foundation (RUG2015-7235); and performed contract research studies with Rodin Therapeutics, Lysosomal Therapeutics Inc., Hoffmann-La Roche Ltd., and Ionis Pharmaceuticals, made available to the institution outside the submitted work. Geke Hospers holds a consulting and advisory role for Amgen, Roche, MSD, BMS, Pfizer, and Novartis and received grants from BMS and Seerave, made available to the institution outside the submitted work. Frederik Cleeren is a postdoctoral fellow of FWO (12R3119N). This research received support from Research Foundation–Flanders (FWO) (G0D8817N). No other potential conflict of interest relevant to this article was reported.

KEY POINTS

QUESTION: What are the in vitro and in vivo characteristics of 2 radiolabeled IL2 variants, ^{18}F-AlF-RESCA-IL2 and ^{68}Ga-Ga-NODAGA-IL2, compared with ^{18}F-FB-IL2?

PERTINENT FINDINGS: Production is faster for these tracers than for the previously developed ^{18}F-FB-IL2. ^{18}F-AlF-RESCA-IL2 shows the best in vitro binding characteristics. In vivo studies showed high ^{18}F-AlF-RESCA-IL2 uptake in PBMCs and lymphoid organs such as spleen, bone marrow, and lymph nodes.

IMPLICATIONS FOR PATIENT CARE: Our results indicate the potential to use ^{18}F-AlF-RESCA-IL2 in future molecular imaging studies for detection of CD25-positive immune cells.

REFERENCES

1. Tumeh PC, Radu CG, Ribas A. PET imaging of cancer immunotherapy. *J Nucl Med.* 2008;49:865–868.
2. van der Veen EL, Bensch F, Glaudemans AWJM, Lub-de Hooge MN, de Vries EGE. Molecular imaging to enlighten cancer immunotherapies and underlying involved processes. *Cancer Treat Rev.* 2018;70:232–244.
3. Boyman O, Sprent J. The role of interleukin-2 during homeostasis and activation of the immune system. *Nat Rev Immunol.* 2012;12:180–190.
4. Liao W, Lin J, Leonard WJ. Interleukin-2 at the crossroads of effector responses, tolerance, and immunotherapy. *Immunity.* 2013;38:13–25.
5. Ross SH, Cantrell DA. Signaling and function of interleukin-2 in T lymphocytes. *Annu Rev Immunol.* 2018;36:411–433.
6. Abbas AK, Trotta E, Simeonov D, Marson A, Bluestone JA. Revisiting IL-2: biology and therapeutic prospects. *Sci Immunol.* 2018;3: eaat1482.
7. Signore A, Annovazzi A, Barone R, et al. ^{99m}Tc-interleukin-2 scintigraphy as a potential tool for evaluating tumor-infiltrating lymphocytes in melanoma lesions: a validation study. *J Nucl Med.* 2004;45:1647–1652.
8. Signore A, Picarelli A, Annovazzi A, et al. ^{123}I-interleukin-2: biochemical characterization and in vivo use for imaging autoimmune diseases. *Nucl Med Commun.* 2003;24:305–316.
9. Loose D, Signore A, Staelens L, et al. ^{123}I-interleukin-2 uptake in squamous cell carcinoma of the head and neck carcinoma. *Eur J Nucl Med Mol Imaging.* 2008; 35:281–286.
10. Di Gialleonardo V, Signore A, Glaudemans AW, Dierckx RA, De Vries EFN. N-(4-^{18}F-fluorobenzoyl)interleukin-2 for PET of human-activated T lymphocytes. *J Nucl Med.* 2012;53:679–686.
11. Di Gialleonardo V, Signore A, Willemsen AT, Sijbesma JW, Dierckx RA, de Vries EF. Pharmacokinetic modelling of N-(4-[^{18}F]fluorobenzoyl)interleukin-2 binding to activated lymphocytes in an xenograft model of inflammation. *Eur J Nucl Med Mol Imaging.* 2012;39:1551–1560.
12. Hartimath SV, Draghiciu O, van de Wall S, et al. Noninvasive monitoring of cancer therapy induced activated T cells using [^{18}F]FB-IL-2 PET imaging. *OncoImmunology.* 2016;6:e1248014.
13. van der Veen EL, Antunes IF, Maarsingh P, et al. Clinical-grade N-(4-[^{18}F] fluorobenzoyl)-interleukin-2 for PET imaging of activated T-cells in humans. *EJNMMI Radiopharm Chem.* 2019;4:15.
14. McBride WJ, Sharkey RM, Goldenberg DM. Radiofluorination using aluminum-fluoride (Al^{18}F). *EJNMMI Res.* 2013;3:36.
15. Cleeren F, Lecina J, Bridoux J, et al. Direct fluorine-18 labeling of heat-sensitive biomolecules for positron emission tomography imaging using the Al^{18}F-RESCA method. *Nat Protoc.* 2018;13:2330–2347.
16. Cleeren F, Lecina J, Ahamed M, et al. Al^{18}F-labeling of heat-sensitive biomolecules for positron emission tomography imaging. *Theranostics.* 2017;7:2924–2939.
17. Velikyan I, Beyer GJ, Långström B. Microwave-supported preparation of ^{68}Ga bioconjugates with high specific radioactivity. *Bioconjug Chem.* 2004;15:554–560.
18. Nagengast WB, de Vries EG, Hospers GA, et al. In vivo VEGF imaging with radiolabeled bevacizumab in a human ovarian tumor xenograft. *J Nucl Med.* 2007;48:1313–1319.
19. Dijkers EC, Kosterink JG, Rademaker AP, et al. Development and characterization of clinical-grade ^{89}Zr-trastuzumab for HER2/neu immunoPET imaging. *J Nucl Med.* 2009;50:974–981.
20. Eisenwiener KP, Prata MI, Buschmann I, et al. NODAGATOC, a new chelator-coupled somatostatin analogue labeled with [$^{67/68}$Ga] and [^{111}In] for SPECT, PET, and targeted therapeutic applications of somatostatin receptor (hsst2) expressing tumors. *Bioconjug Chem.* 2002;13:530–541.
21. Novy Z, Stepankova J, Hola M. el al. Preclinical evaluation of radiolabeled peptides for PET imaging of glioblastoma multiforme. *Molecules.* 2019;24:2496.
22. Cleeren F, Lecina J, Billaud EMF, Ahamed M, Verbruggen A, Bormans GM. New chelators for low temperature Al^{18}F-labeling of biomolecules. *Bioconjug Chem.* 2016;27:790–798.
23. Chianelli M, Signore A, Fritzberg AR, Mather SJ. The development of technetium-99m-labelled interleukin-2: a new radiopharmaceutical for the in vivo detection of mononuclear cell infiltrates in immune-mediated diseases. *Nucl Med Biol.* 1997;24:579–586.
24. Karczmarczyk U, Garnuszek P, Maurin M, et al. Investigation of ^{99m}Tc-labelling of recombinant human interleukin-2 via hydrazinonicotinamide. *Nucl Med Biol.* 2010;37:795–803.
25. D'Alessandria C, Di Gialleonardo V, Chianelli M, et al. Synthesis and optimization of the labeling procedure of ^{99m}Tc-HYNIC-interleukin-2 for in vivo imaging of activated T lymphocytes. *Mol Imaging Biol.* 2010;12:539–546.
26. Signore A, Chianelli M, Toscano A, et al. A radiopharmaceutical for imaging areas of lymphocytic infiltration: ^{123}I-interleukin-2—labelling procedure and animal studies. *Nucl Med Commun.* 1992;13:713–722.
27. Glaudemans AW, Bonanno E, Galli F, et al. In vivo and in vitro evidence that ^{99m}Tc-HYNIC-interleukin-2 is able to detect T lymphocytes in vulnerable atherosclerotic plaques of the carotid artery. *Eur J Nucl Med Mol Imaging.* 2014;41: 1710–1719.
28. Signore A, Chianelli M, Annovazzi A, Bonanno E. ^{123}I-interleukin-2 scintigraphy for in vivo assessment of intestinal mononuclear cell infiltration in Crohn's disease. *J Nucl Med.* 2000;41:242–249.
29. Markovic SN, Galli F, Suman VJ, et al. Non-invasive visualization of tumor infiltrating lymphocytes in patients with metastatic melanoma undergoing immune checkpoint inhibitor therapy: a pilot study. *Oncotarget.* 2018;9:30268–30278.
30. Tavaré R, McCracken MN, Zettlitz KA, et al. Engineered antibody fragments for immuno-PET imaging of endogenous CD8+ T cells in vivo. *Proc Natl Acad Sci USA.* 2014;111:1108–1113.
31. Tavaré R, McCracken MN, Zettlitz KA, et al. Immuno-PET of murine T cell reconstitution postadoptive stem cell transplantation using anti-CD4 and anti-CD8 cys-diabodies. *J Nucl Med.* 2015;56:1258–1264.
32. Tavaré R, Escuin-Ordinas H, Mok S, et al. An effective immuno-PET imaging method to monitor CD8-dependent responses to immunotherapy. *Cancer Res.* 2016;76:73–82.
33. Rashidian M, Ingram JR, Dougan M, et al. Predicting the response to CTLA-4 blockade by longitudinal noninvasive monitoring of CD8 T cells. *J Exp Med.* 2017;214:2243–2255.